Heel Ulcers: Investigating Injurious Tissue Load-Thresholds in Humans, Based on a Patient- Specific Computational Heel Model

Rinat Friedman, Noga Shabshin, Yohan Payan, Amit Gefen

Heel Ulcers: Investigating Injurious Tissue Load-Thresholds in Humans, Based on a Patient-Specific Computational Heel Model

Rinat Friedman[a], Noga Shabshin[b,c], Yohan Payan[d], Amit Gefen[a]

[a] Department of Biomedical Engineering, Faculty of Engineering, Tel Aviv University, Israel

[b] HaEmek Medical Center, Israel

[c] Hospital of the University of Pennsylvania, Penn Medicine, USA

[d] Laboratoire TIMC-IMAG, CNRS & University Grenoble Alpes, France

***Corresponding author:**

Amit Gefen, Ph.D.
Professor of Biomedical Engineering
The Herbert J. Berman Chair in Vascular Bioengineering

Department of Biomedical Engineering
Faculty of Engineering
Tel Aviv University
Tel Aviv 69978, Israel
Fax: +972-3-6405845
E-mail: gefen@tauex.tau.ac.il

Published in the book:

Innovations and Emerging Technologies in Wound Care

Editor: **Professor Amit Gefen**

Abstract

Heel ulcer (HU) is the second most common type of ulcer, formed when the skin and fat that envelope the calcaneus are deformed for extended periods between the bone and a support, eventually causing structural damage to the tissues. No specific data exist regarding the in-vivo mechanical stress and strain thresholds for the onset and progression of HUs within clinically-relevant time periods (e.g., while anesthetized in the operation room, bed-bound in nursing homes, etc.).

We used an MRI heel scan of a 72 years-old male with a clearly demonstrated deep tissue injury at the right heel, to develop a three-dimensional finite element model of the heel which include the calcaneal bone, subcutaneous fat, insertion and distal region of the Achilles tendon, and the skin. Biomechanical properties of all tissues were adopted from the literature. A pre-injury anatomy was simulated using healthy-tissue mechanical attributes.

Thresholds of the mechanical loads which led to the onset and progression of HU were accessed by back-calculating the mechanical conditions in the wound, caused by the foot weight, as it is not expected to significantly change during the injury-relevant time frame. Shear due to support inclination and foot weight were simulated by displacing the superior surface of the calcaneus downward and horizontally.

Von-Mises stress and Lagrangian strain injury thresholds were offered, along with compressive to tensile proportions of the total strain. The influence of shear stress, foot weight, and bed-angle on the thresholds was analyzed. Strain energy density was examined as a predictor for ulcer formation.

Keywords: *Heel ulcer, Ulcer injury thresholds, Finite elements, Computer simulations*

1. Introduction

A pressure ulcer (PU) is an injury to the skin and/or underlying tissues pressed against a bony prominence, due to continuous pressure and shear forces [1]. Deep tissue injuries (DTIs)[1] might become life-threatening and can ultimately result in death [2, 3]. Mortality likelihood is increased almost by two in bed-bound patients with PUs, compared to bed-bound patients without them [4]. PUs prolong healing processes of other principal conditions, lengthen hospitalization [3, 5], and carry immense healthcare costs. It was previously reported that approximately 1.6 million PUs occurred yearly in US hospitals alone, with a total cost of 2.2-3.6 billion dollars. On average, DTIs increased healthcare costs per patient by 14-23 thousand dollars [5].

The heel is the second most common location for heel ulcers (HUs), occurring in 26% of all ulcer cases, and has the second highest percentage (38.5%) of DTIs [6]. HUs are formed when the soft tissues of the posterior heel (thin layers of skin and subcutaneous fat) are subjected to sustained deformations while the foot is weight-bearing.

When in a supine position due to lengthy surgical procedures, long-term hospitalization, paralysis, or spinal cord injury, the soft tissues of the posterior heel are deformed by the weight of the foot when pressed between the rigid surface of the posterior calcaneus and the support surface [3, 7, 8, 9]. Consequently, ischemia is formulated, rapidly leading to tissue deterioration and ultimately resulting in an ulceration of the area [10, 2].

Compressive and tensile stresses and strains are the primary mechanical factors for the formation of ulcers of all severities. Friction is considered a secondary contributing factor [11, 12, 13]. Shear and tensile stresses will occur around the pressure point even for a completely

List of abbreviations used in the text: HU – heel ulcer; PU – pressure ulcer, DTI – deep tissue injury; FW – foot weight, BW – body weight, FE – finite element, 3D – three dimensional

perpendicular pressure [12]. This reaction is heightened around a bony prominence that acts as a peg around which the tissue is stretched and distorted [12, 13].

Tissue distortion is formulated by shear and pressure stresses that entrap the tissue between an external support (e.g., a mattress) and an internal reaction surface (e.g., bone), which causes stretching or compression of blood vessels in the tissue, leading to vessels ischemia that results in necrosis of the tissue [11, 13, 14].

Friction promotes occurrence of shear stresses, thus stimulates the formation of ulcers. As the outer surface skin is kept immobilized against the support while the body keeps moving, a relative motion is produced between the skin and the rest of the body. This is a form of the "hammock effect" with the outer layer of the skin acting as the "tight cover". This relative motion of tissues leads to inter-tissue shear stresses and lateral strains which result in ulcer formation [12, 13].

The primary objectives of this study are: (1) Develop a three-dimensional (3D) computational, FE modeling of a heel affected by a HU, based on a real case of HU, scanned by MRI. (2) Use the 3D model to investigate the case retrospectively and determine the thresholds of internal mechanical loads in skin and fat, which led to the onset and development of the HU in this case. (3) Effective (von-Mises) stress, effective (Lagrangian) strain and strain energy density are scalar parameters that can be computed by Finite Element (FE) analysis and that are commonly used to evaluate the influence of external loads on biological tissues [15, 16, 17, 18, 19]. Our third goal was to evaluate the best parameter out of the three for one-to-one indication of injury.

2. Methods

2.1. Geometry

In this study we used an MRI scan of a 72 years old male subject (bodyweight = 95kg) with a set of 41 T2-weighted 3mm-spaced images, portraying an axial cut of the right foot. The calcaneus, fat, skin, Achilles tendon tissues are demonstrated in the scan. A DTI with ulcerated skin and subcutaneous fat tissue is clearly visible in the scan (Figure 1), located on the posterior side of the heel, above the Achilles tendon insertion, which is typical for HUs that develop following a prolonged supine position (Figure 1, a-b). The analysis of the MRI data were conducted in close collaboration with an expert radiologist with specialization in detecting soft tissue damage by means of MRI, Dr. Nogah Shabshin from HaEmek Medical Center in Israel and the Hospital of the University of Pennsylvania in the US.

2.2. Finite element modeling

The MRI images were segmented into masks, representing each of the tissues included in the scan. Simpleware ScanIP (Version 6) was used for the creation and meshing of the 3D model. All masks closely followed the MRI scan and were given physiological geometry (size and shape) while the ulcer region was replaced with healthy tissue structures (Figure 1, c-e). Number and type of mesh elements for each tissue are descried in Table 1. The heel was rested on a support with different stiffness levels and angles. The stress and strain levels which formed due to the foot weight were then calculated in the original ulcer site. Von-Mises (effective) stress, shear stress, and Lagrangian strains were used for calculating the loading applied on the soft tissues of the heel in the subsequent injured area.

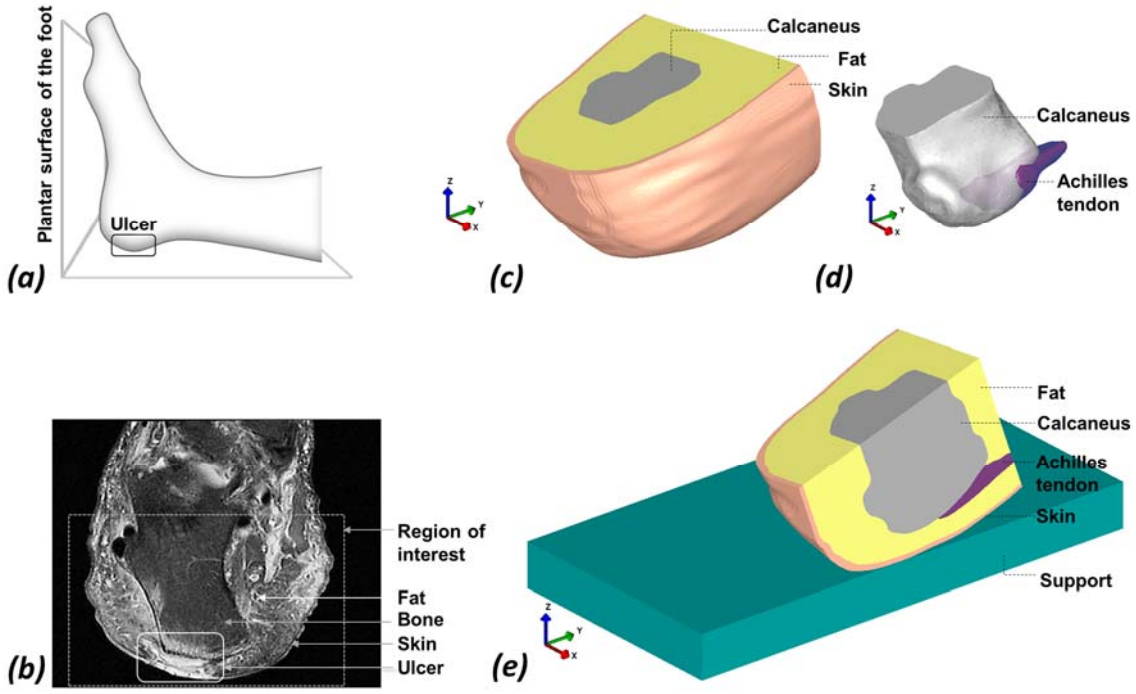

---Figure 1---

The model was solved using the FEBio Software Suite (University of Utah, US). PreView (ver. 1.18.2) was used for assigning material properties, boundary conditions, and model forces, as detailed in the following segments. PreView was also used for building and meshing the support surface ("mattress"). FEbio (ver 2.3.1) was used for numerical calculations and PostView (ver. 1.9.1) for force, stress, and strain analysis.

2.3. Mechanical Properties

All tissues were assigned physiological mechanical properties according to the literature (Table 1). The skin was assigned "aged" mechanical properties according to [20]. The skin, fat and Achilles tendon were assigned nearly incompressible biophysical properties, due to their high water contents [20, 21]. Mechanical behavior of skin and fat was described using a Neo-Hookean model for isotropic hyperelastic materials [20, 21]:

$$[1]\ W = \frac{G_{ins}}{2}(\lambda_1^2 + \lambda_2^2 + \lambda_3^2 - 3) + \frac{1}{2}K(lnJ)$$

where W is the strain energy function, G_{ins} is the shear modulus, λ_i are the principal stretch ratios, K is the bulk modulus of the tissue, and J the determinant of the deformation gradient tensor. The calcaneus was considered an isotropic linear elastic solid [21].

For the intensions of this study and based on previous relevant works [20, 21], elastic component of skin and fat was considered to be isotropic. The Achilles tendon retains transversely isotropic and linearly elastic properties when compressed perpendicularly to the main fiber axis [22], which was the case in this work and so it was treated as an uncompressible isotropic elastic material [3]. Tendon's elastic modulus was taken as a mean between E_{11}, E_{22} for median strain condition from [22], and maximal E for moderate compression from [23]. Tissue properties used in the model are summarized in Table 1.

Table 1 -Tissue mechanical properties and number of element that were used in the model. (*) A rather high value for the elastic modulus of the skin was chosen according to *[20]*. Values in the range of E=1MPa for old skin tissue, were also reported in other sources *[24, 25, 26]*

Tissue	Number of mesh elements	Type of mesh elements	Shear Modulus, G_{ins} [MPa]	Bulk Modulus, K [MPa]	Poisson's Ratio, υ	Elastic Modulus, E [MPa]	Source
Skin	83,387	4-node linear tetrahedron	0.3247	32.357	0.495	0.970853*	[20]
Fat	213,170		0.000286	0.0285	0.495	0.000855	[20]
Bone	65,971		-	-	0.3	7000	[20, 21]
Achilles	31,646		-	-	0.495	0.1945	[22, 23]

Mechanical properties of the support surface were chosen to be lineal elastic with elastic moduli of 40, 60, 80, 100 kPa, based on our previous work which described elastic moduli and stiffness behavior for hospital mattresses [27, 21, 28]. The support was meshed with 8-node linear hexahedrons.

2.4. Boundary conditions

The bottom plane of the support was immobilized for translation and rotation motions in all directions. Static friction coefficient between heel and support was adopted from the literature [21]. As patient's precise foot weight was not known, anthropometric data (foot weight as % of total body weight) was used [29], indicating that foot weight is approximately 1.458±0.126% of the total body weight. Two foot weights were modeled, accounting for a "light" and a "heavy" foot: 9.3N (1% of body weight) and 20.6N (2.2% of body weight), accordingly. The superior surface of the calcaneus was displaced downward and horizontally, to simulate the load of the foot weight. Since contact force is equal to the foot weight while resting on a support, the load levels were confirmed by verifying the contract force between the heel and the mattress for each case. Light and heavy foot weights were simulated by adding additional displacement of the calcaneus, without changing the width of the fat or skin layers, so the original geometry portrayed by the MRI reminded intact.

The foot was set in three mattress positions according to common surgical bed positions: Trendelenburg (Figure 2.a), horizontal (Figure 2.b), and revere Trendelenburg (Figure 2.c). Several angles were simulated for the Trendelenburg and reverse Trendelenburg positions: 0^o (horizontal), 5^o, 10^o, 20^o, and 30^o, chosen according to standard surgical bed angle-range and common surgical practices for procedures requiring a non-horizontal patient position [30, 31, 32, 33, 34, 35, 36, 37].

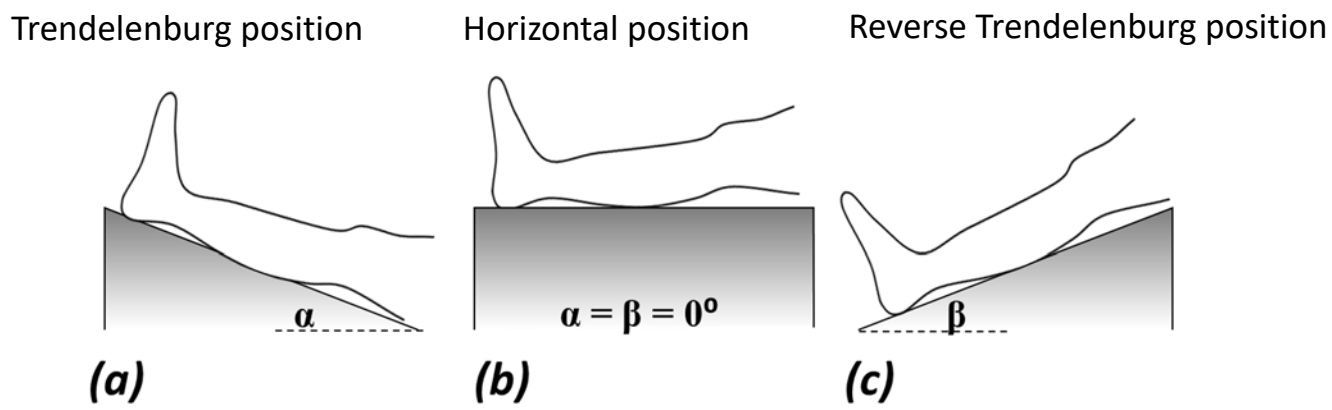

--- Figure 2 ---

2.5. Outcome Measures

The skin and fat in original HU area were analyzed for effective stresses and Lagrangian strains. Outcome measures included: maximal effective (von-Mises) stress, maximal shear stress, and maximal Lagrangian strains. Outcome measures were compared between the various support angles and between fat and skin for each angle. In several cases (partial angles/mattress stiffness) additional measures included: maximal compressive and tensile strains, and distribution of strain energy density.

3. Results

An example of the FE model of the heel is presented in Figure 3, rested on a horizontal 80kPa support. Colors indicate the effective stress, Lagrangian strain and strain energy density distribution. The original wound area is marked, clearly indicating the subsequent deep tissue injury was a site for stress and strain concentration. A close-up of the loaded tissues in the wound area is also presented (Figure 3.d).

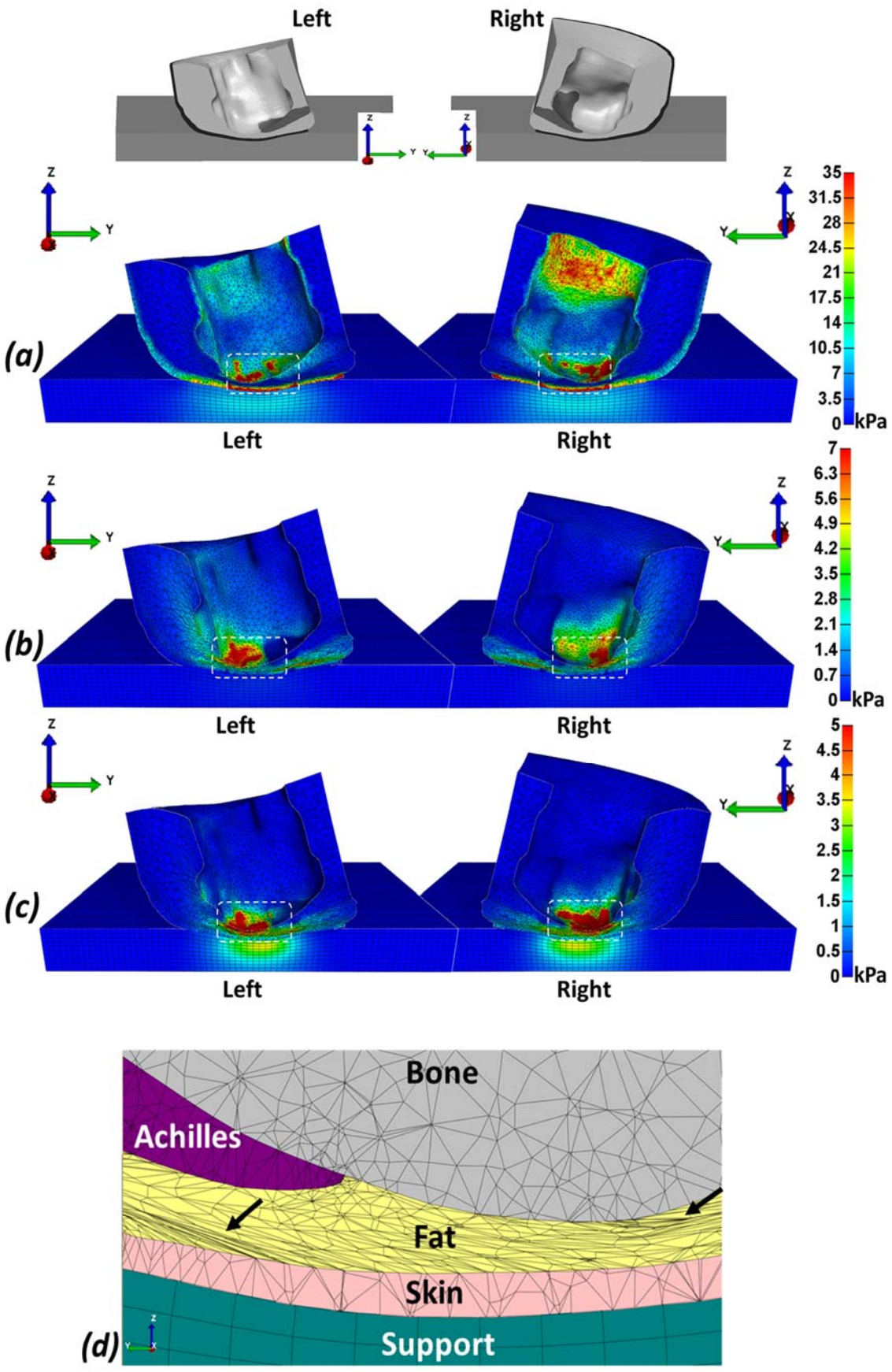
Left
Right
(a)
35
31.5
28
24.5
21
17.5
14
10.5
7
3.5
0
kPa
Left
Right
(b)
7
6.3
5.6
4.9
4.2
3.5
2.8
2.1
1.4
0.7
0
kPa
Left
Right
(c)
5
4.5
4
3.5
3
2.5
2
1.5
1
0.5
0
kPa
Left
Right
Bone
Achilles
Fat
Skin
Support
(d)

--- Figure 3 ---

Computational data were cross-examined by category using graphs and tables so that large amount of data could be inspected simultaneously. In certain categories some data were not considered for efficacy purposes, when no further conclusions could be drawn from it. For convenience, the angle-range of the Trendelenburg position is marked by α, and the angle-range of reverse Trendelenburg position is marked by β. The abbreviation "FW", used in the following figures, stands for "Foot Weight". For example, FW = 2.2%BW signifies that the Foot Weight is 2.2% of the total body weight.

Main results for effective and shear stress as function of tissue type (fat/skin), support angles and mattress stiffness levels, are presented in Figure 4. A clear lineal connection between support stiffness stress levels is evident (Figure 4, a-b), in addition to higher stress levels in the skin as opposed to the fat (Figure 4, e-h).

Going from a 40kPa mattress to a 100 kPa support, both the maximal effective and shear stresses were increased by more than 30% in the skin, and more than doubled their values in the fat. Maximal shear stress was about 55% of the total maximal effective stress in both skin and fat, regardless of the angle. Results for α and β angles are summarized in Table 2.

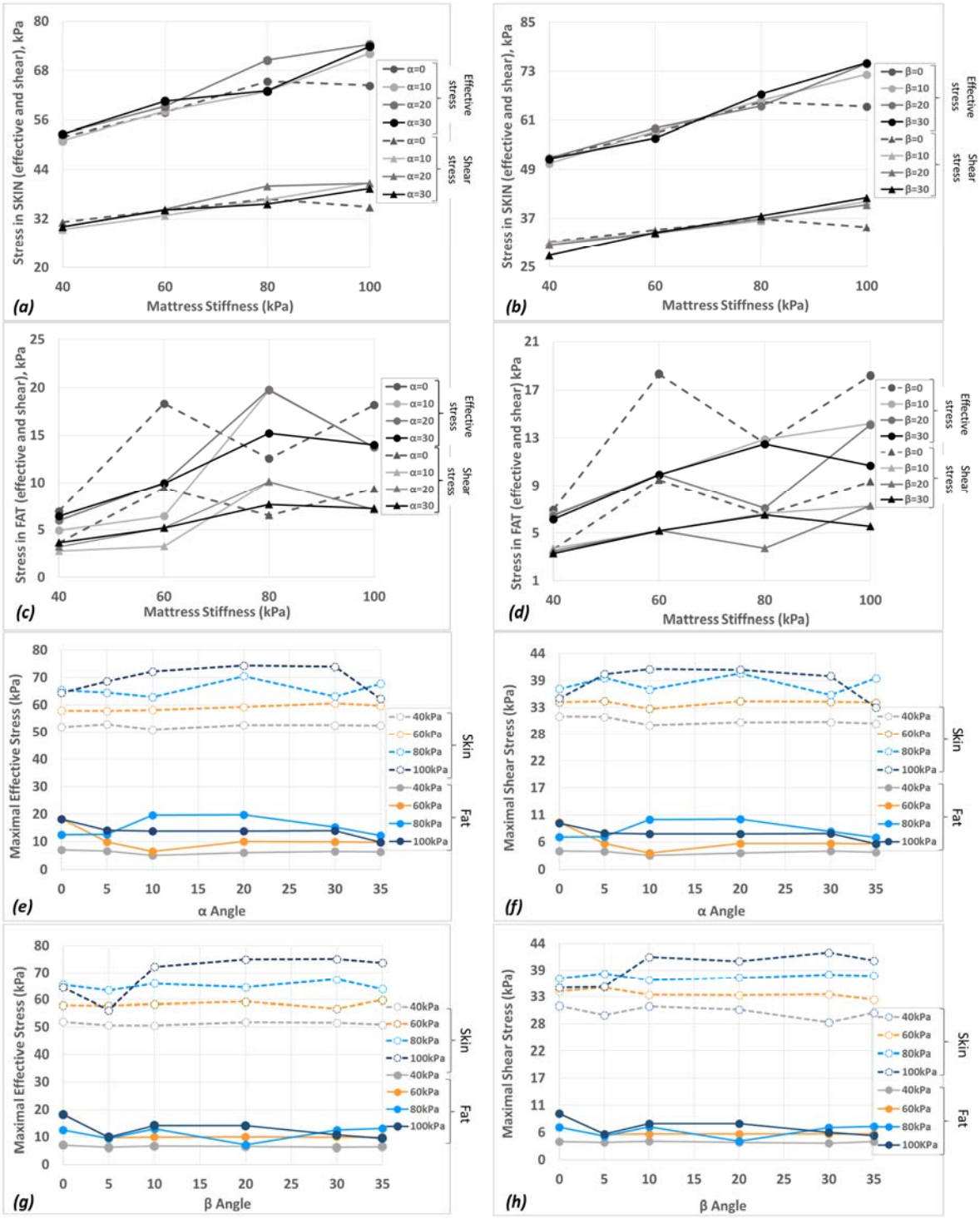
Stress in SKIN (effective and shear), kPa
Mattress Stiffness (kPa)
(a)
α=0
α=10
α=20
α=30
Effective stress
Shear stress
Stress in SKIN (effective and shear), kPa
Mattress Stiffness (kPa)
(b)
β=0
β=10
β=20
β=30
Effective stress
Shear stress
Stress in FAT (effective and shear), kPa
Mattress Stiffness (kPa)
(c)
α=0
α=10
α=20
α=30
Effective stress
Shear stress
Stress in FAT (effective and shear) kPa
Mattress Stiffness (kPa)
(d)
β=0
β=10
β=20
β=30
Effective stress
Shear stress
Maximal Effective Stress (kPa)
α Angle
(e)
40kPa
60kPa
80kPa
100kPa
Skin
Fat
Maximal Shear Stress (kPa)
α Angle
(f)
40kPa
60kPa
80kPa
100kPa
Skin
Fat
Maximal Effective Stress (kPa)
β Angle
(g)
40kPa
60kPa
80kPa
100kPa
Skin
Fat
Maximal Shear Stress (kPa)
β Angle
(h)
40kPa
60kPa
80kPa
100KPa
Skin
Fat

--- Figure 4 ---

Table 2 - Maximal shear and effective stresses (averaged values for all α values and all β values) increase percentage, in skin and in fat, when going from a 40kPa mattress to a 100 kPa mattress. Maximal shear stress as percentage of the total maximal effective stress, for α and β angles, for skin and fat.

Tissue	Maximal effective stress increase in %		Maximal shear stress increase in %		Maximal shear stress as % of total maximal effective stress	
	(α)	(β)	(α)	(β)	(α)	(β)
Skin	35%	34%	29%	29%	57.2%	57.6%
Fat	139%	108%	128%	97%	52.3%	52.5%

We introduce what we call "injury thresholds", calculated for skin and fat tissue for low (FW1%BW) and high (FW2.2%BW) foot weight. Effective and shear stress injury thresholds were calculated using the average maximal effective and shear stresses and vary as function of mattress stiffness. Complete injury thresholds in kPa are described in [Table 3].

Table 3 - Injury thresholds (kPa) in the skin (I) and fat (II): (FW1%BW - FW2.2%BW). Thresholds vary for each mattress stiffness. Effective stress injury thresholds for α and β angles are indicated by "Effective stress (α)" and "Effective stress (β)", respectively. Shear stress injury thresholds for α and β angles are indicated by "Shear stress (α)" and "Shear stress (β)", respectively.

(I)	Skin injury thresholds (FW1%BW – FW2.2%BW), kPa			
Mattress stiffness (kPa)	Effective stress (α)	Effective stress (β)	Shear stress (α)	Shear stress (β)
40	48 - 52	48 - 51	27 - 30	27 - 30
60	55 - 59	55 - 58	32 - 34	32 - 34
80	48 - 66	61 - 65	35 – 38	35 - 37
100	62 - 69	62 - 69	36 – 38	35 - 37
(II)	**Fat injury thresholds (FW1%BW – FW2.2%BW), kPa**			
Mattress stiffness (kPa)	**Effective stress (α)**	**Effective stress (β)**	**Shear stress (α)**	**Shear stress (β)**
40	3 - 6	3 - 6	2 - 3	2 - 4

60	4 - 11	4 - 11	2 - 6	2 - 6
80	4 - 15	4 - 11	2 - 8	2 - 6
100	4 - 15	4 - 13	2 - 7	2 - 7

The main results for Lagrangian strain injury thresholds for fat and skin, as function of support stiffness levels [Figure 5] and angles [Figure 6], are presented next. A clear lineal increase of strain in the skin as function of mattress stiffness is evident [Figure 5, a-b]. However, strain levels in the fat show a far lesser correlation with mattress angles and stiffness [Figure 5, c-d; Figure 6].

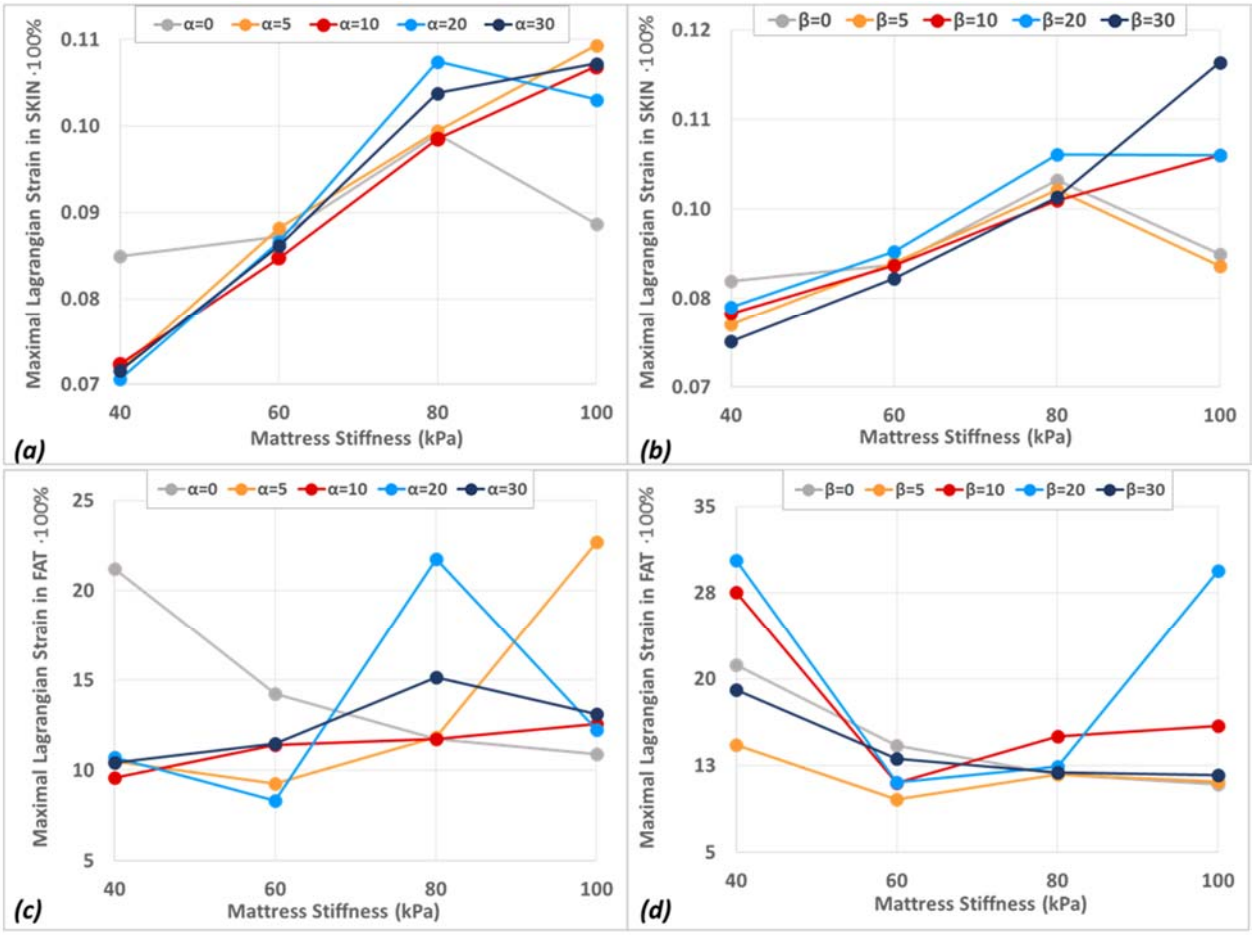

Figure 5

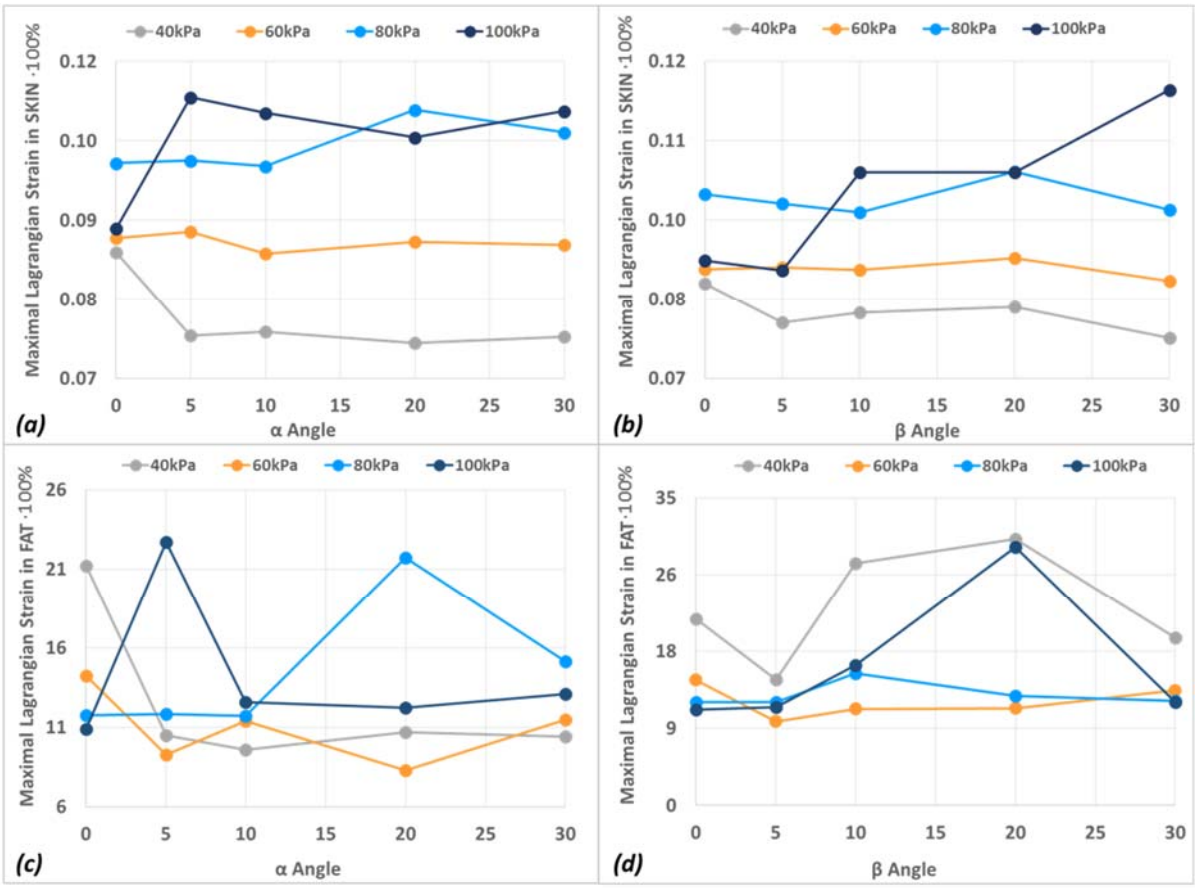

---Figure 6---

Lagrangian strain injury thresholds in skin and fat are presented in Table 4 for α and β angles, in addition to threshold levels averaged for all the angles for each mattress stiffness. It is evident that strain levels in the skin are much lower than in the fat tissue, with the difference escalating as the weight of the foot increases [Table 5].

Table 4 - (a) Injury thresholds for Lagrangian strain is skin and fat (b) Threshold levels of strain, averaged for all the angels for each mattress stiffness.

Mattress stiffness (kPa)	Skin - injury thresholds Strain (·100%) (FW1%BW – FW2.2%BW)		Fat - injury thresholds Strain (·100%) (FW1%BW – FW2.2%BW)		Skin - injury thresholds AVERAGE of all angles Strain (·100%) (FW1%BW – FW2.2%BW)	Fat - injury thresholds AVERAGE of all angles Strain (·100%) (FW1%BW – FW2.2%BW)
	(α)	(β)	(α)	(β)		
	0.08 - 0.09	0.08 - 0.09	7 - 30	7 - 21	0.08 - 0.09	7 - 26

60	0.08 - 0.09	0.08 - 0.09	6 - 14	6 - 14	0.08 - 0.09	6 - 14
80	0.09 - 0.10	0.09 - 0.09	6 - 15	6 - 22	0.09 - 0.10	6 - 18
100	0.10 - 0.12	0.11 - 0.11	11 - 29	9 - 23	0.10 - 0.11	10 - 26

Table 5 - Number of times Maximal Lagrangian strain in fat is larger than in skin, as function of foot weight - low (BW = 1%) and high (BW = 2.2%), and as function of support stiffness (e.g. for 1%BW and a 40kPa mattress, the Maximal Lagrangian strain in fat is 88 times larger than in skin, and for 60kPa mattress Maximal Lagrangian strain in fat is 70 times larger than in skin).

Foot weight as % of body weight	**Mattress Stiffness(kPa)**				**Average for all stiffnesses**
	40	**60**	**80**	**100**	
FW is 1%BW	88	70	60	97	79
FW is 2.2%BW	303	161	193	232	222

Lagrangian strain is composed of compressive (vertical) and tensile (lateral) strains, the division between which was examined for skin and fat for several select support configurations, as described in [Table 6].

Table 6 - Transverse stretch as % of total strain vs. vertical compression as % of total strain. Only two angles were examined: β=0 and β=30.

Tissue	**Angle**	**Foot Weight**	**Mattress stiffness (kPa)** Stretch% of total strain - Compression% of total strain		
			40	**60**	**80**
Skin	β=0	1%BW	48% - 52%	49% - 51%	51% - 49%
		2.2%BW	51% - 49%	49% - 51%	50% - 50%
	β=30	1%BW	50% - 50%	49% - 51%	50% - 50%
		2.2%BW	52% - 48%	54% - 46%	50% - 50%
Fat	β=30	1%BW	89% - 11%	88% - 12%	85% - 15%
		2.2%BW	95% - 5%	91% - 9%	93% - 7%

	β=30	1%BW	100% - 0%	87% - 13%	93% - 7%
		2.2%BW	99% - 1%	92% - 8%	95% - 5%

Strain energy density distribution was analyzed graphically: a single and distinct zone of maximal strain energy density in the heel model is located directly in the middle of the eventual ulcer location, as opposed to effective stress. This is demonstrated in Figure 7.

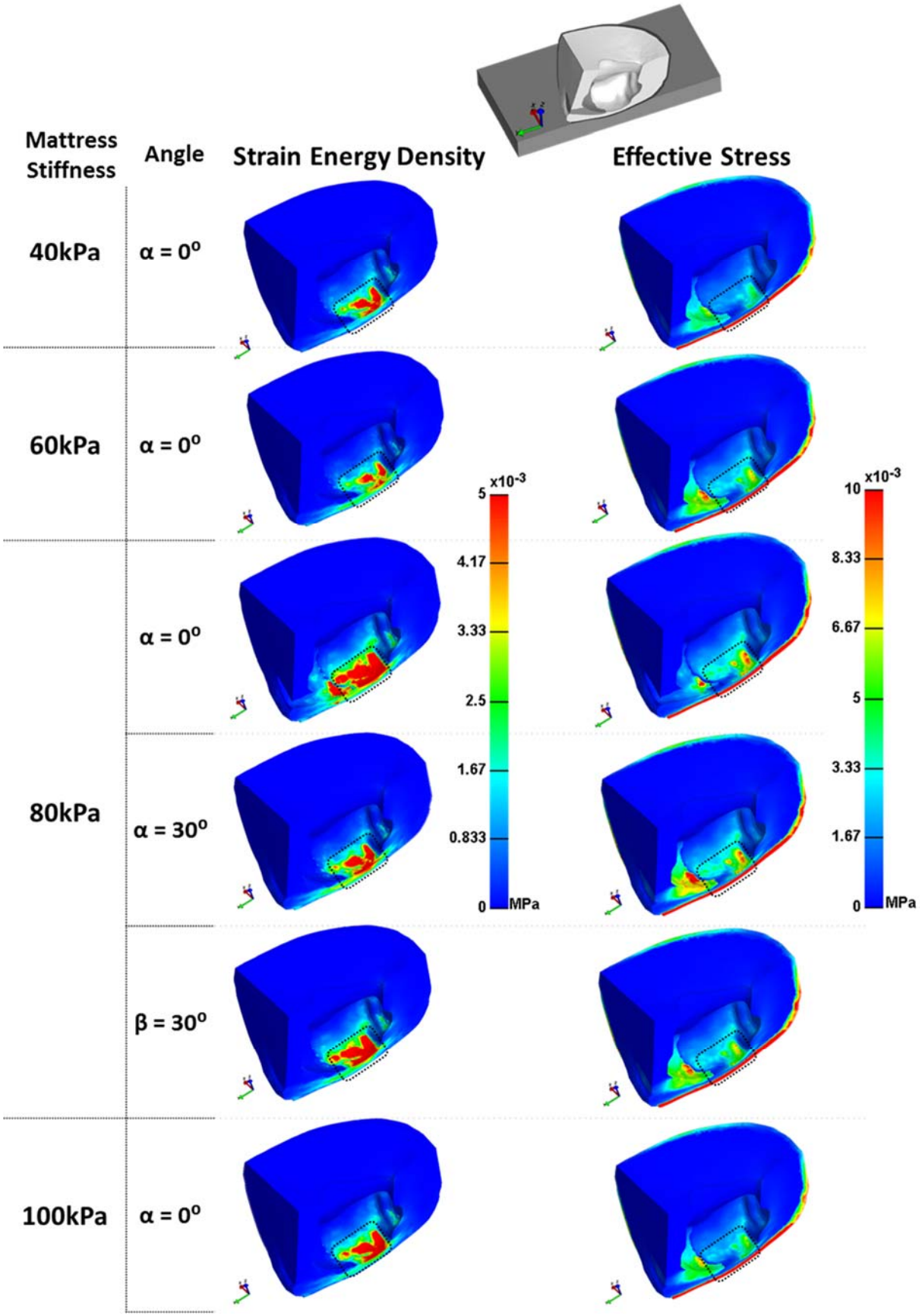
Mattress Stiffness
Angle
Strain Energy Density
Effective Stress
40kPa
α = 0°
60kPa
α = 0°
80kPa
α = 0°
α = 30°
β = 30°
100kPa
α = 0°
x10-3
5
4.17
3.33
2.5
1.67
0.833
0
MPa
x10-3
10
8.33
6.67
5
3.33
1.67
0
MPa

---Figure 7---

4. Discussion

An MRI scan of the right heel of a 72 year old male subject, with a pre-existing DTI at the time of the scan, was used to create patient-specific 3D FE model of the heel that included the calcaneus, Achilles tendon, fat, and skin. The original DTI area was given properties of healthy tissues. Foot weight related tissue loads that acted in the original wound area and which instigated HU formation were calculated and used to determine suggested injury thresholds. Since foot weight was not expected to drastically change during the injury-time frame (hour to days) of the patient's hospitalization, the load levels acting in the DTI area were also expected to remain mostly unvarying. We concluded that the computed stress and strain levels in the simulation (during the "healthy" state) would have been the same later on, when the ulcer was formed. This allowed us to estimate injury-causing stress and strain thresholds, as described in Tables 5-8. Over time, these load levels are expected to result in a DTI.

The fat tissue has exhibited effective and shear stress injury thresholds 14 to 6 and 16 to 6 times lower (for high and low foot weights), accordingly, compared to the skin, regardless of mattress stiffness and angle. This suggests the fat is much more susceptible to stress than the skin, since a lower stress is needed for injuring this tissue, possibly clarifying why ulcer onset is often initiated in the fat.

These results also exhibit the pivotal role shear stress has in ulcer formation, with the shear component of the total effective stress being larger than 50% for skin and fat for both angles, as demonstrated in Table 2.

The results indicate that fat tissue has a much greater tolerance to strain than the skin, as strain levels in the fat were 80 to 220 times higher than in the skin, for all foot weights, angles, and support stiffnesses.

Effective stress injury thresholds were significantly influenced by mattress stiffness. When going from a 40kPa to a 100kPa mattress, effective stress and shear stress injury thresholds in the skin increased by 30% for both the “light” and “heavy” foot, and by 30% and 110% in the fat for the “light” and “heavy” foot, accordingly.

Strain injury thresholds in the skin were significantly influenced by mattress stiffness, on average rising by 25% when going from a 40kPa support to a 100kPa support, with the highest strain levels resulting for the softest mattress (40kPa). Foot weight increase from 1%BW to 2.2%BW, caused strain injury thresholds of fat to triple for 80kPa and 100kPa supports, to double for a 60kPa support and to quadruple for a 40kPa support. Strain injury thresholds of skin were less influenced by the weight increase, increasing by 11.5% on average when going from 1%BW to 2.2%BW. These results indicate that a mattress that is too soft might have a disadvantageous influence on HU formation, by causing greater deformations of soft tissues due to the sinking of the foot inside the mattress, while the friction between the foot and the mattress prevents relative movement of the outer skin layer, thus creating a drag effect of the inner soft tissues and resulting in a “hammock effect” with the skin acting as the “tight cover” [12, 13]. The increase in foot weight had also a significant effect on stress levels, doubling the effective and shear stress levels in the fat for a 40kPa mattress, while only increasing by 10% in the skin. Increasing the foot weight for 60, 80, and 100 kPa supports, caused the stress injury thresholds to rise by 210% on average in the fat, while growing by 10% in the skin.

For all mattresses and angles, distribution of compressive-tensile strains in the skin was equally 50%-50%. However, the fat had mostly experienced tensile strains, with compressive-tensile distribution of 8%-92%. Following the downwards compression due to the weight of the foot, the fat repositioned laterally, rather than actually compress in-place, due to its soft (compared to the skin) but uncompressible nature.

A small angle of 5^{o}-10^{o} reduced effective and shear stress levels in the fat tissue by 25-35% compared to the horizontal position, for both Trendelenburg and reverse Trendelenburg positions and all mattress stiffness levels but the 80 kPa mattress. An angle of 5^{o} had also reduced strain levels for both positions with a 29% drop in the fat and a 4% in the skin, for all support stiffnesses but 100kPa. A 10^{o} angle had not improved strain levels, and in some cased even increased them, leading to the conclusion that a 5^{o}-tilted bed (lifted or lowered), can greatly reduce strain and stress levels in both skin and fat, thus lessening the chances for ulcer formation.

Lastly, a correlation was observed between the eventual ulcer area and areas with distinct concentration of strain energy density, indicating that a high level of strain energy density is a good predicator for ulcer formation, which is also coherent with [19] and confirms the hypothesis suggested by [38], proposing to look at strains values (as opposed to stress values) as a predicator for a pressure ulcer.

The 3D FE modeling of the heel presented in this study has allowed us to gain knowledge upon the stress and strain levels involved in the formation of deep tissue injury of the heel.

We examined the influence of bed angle and foot weight on the resultant stress levels on the skin and fat tissues and determined injurious effective stress and shear stress thresholds. Although this work is based on a single MRI scan set and cannot provide universal deep tissue

injury thresholds, the data offers an initial reference point to the size and range of ulcer causing stress and strain levels.

Acknowledgements

This research was supported by a grant from the Ministry of Science Technology and Space, Israel & the CNRS, PICS program, France (YP, AG). The authors wish to extend their gratitude to the National Pressure Ulcer Advisory Panel (NPUAP) for funding this research with a mini-grant.

5. References

[1] J. Black, M. Baharestani, B. Dorner, L. Edsberg, D. Langemo, M. E. Posthauer, C. Ratliff, G. Taler and National Pressure Ulcer Advisory Panel, "National Pressure Ulcer Advisory Panel's Updated Pressure Ulcer Staging System," *Dermatology Nursing,* vol. 19, no. 4, pp. 343-349, 2007.

[2] E. Fowler, S. Scott-Williams and J. B. McGuire, "Practice Recommendations for Preventing Heel Pressure Ulcers," *Ostomy Wound Management,* vol. 54, no. 10, pp. 42-57, October 2008.

[3] A. Russo, C. Steiner and W. Spector, "Hospitalizations Related to Pressure Ulcers Among Adults 18 Years and Older, 2006 - Statistical Brief #64," *Healthcare Cost and Utilization Project (HCUP) Statistical Briefs,* December 2008.

[4] H. Brem and C. Lyder, "Protocol for the successful treatment of pressure ulcers," *The American Journal of Surgery,* vol. 188, no. 1, Supplement 1, pp. 9-17, July 2004.

[5] S. A. Aronovitch and K. Bechrich, "Hospital-acquired pressure ulcers: a comparison of costs in medical vs. surgical patients," *Nursing Economics,* vol. 17, no. 5, pp. 263-71, 1999.

[6] K. Vanderwee, M. Clark, C. Dealey, L. Gunningberg and T. Defloor, "Pressure ulcer prevalence in Europe: a pilot study," *Journal of Evaluation in Clinical Practice,* vol. 13, no. 2, pp. 227-35, 2007.

[7] C. VanGilder, S. Amlung, P. Harrison and S. Meyer, "Results of the 2008 – 2009 International Pressure Ulcer Prevalence™ Survey and a 3-Year, Acute Care, Unit-Specific Analysis," *Ostomy Wound Manage,* vol. 55, no. 11, pp. 39-55, 2009.

[8] A. Gefen, K. J. Farid and I. Shaywitz, "A Review of Deep Tissue Injury Development, Detection, and Prevention: Shear Savvy," *Ostomy Wound Management,* vol. 59, no. 2, pp. 26-35, 2013.

[9] S. G. Krzysztof, "Pressure ulcer prevention. Part 1. Causes of pressure ulcers.," *Nursing Times,* vol. 98, no. 11, pp. 41-44, 2002.

[10] J. D. Bauer, J. S. Mancoli and L. G. Phillips, "Chapter 74: Pressure Sores," in *Grabb and Smith's Plastic Surgery*, 6th ed., C. H. Thorne, S. P. Bartlett, R. W. Beasley, S. J. Aston, G. C. Gurtner and S. L. Spear, Eds., Lippincott Williams & Wilkins, 2007, pp. 722-729.

[11] A. Gefen, K. J. Farid and I. Shaywitz, "A Review of Deep Tissue Injury Development, Detection, and Prevention: Shear Savvy," *Ostomy Wound Management,* vol. 59, no. 2, pp. 26-35, February 2013.

[12] "International review: Pressure ulcer prevention: pressure, shear, friction and microclimate in context. A consensus document," Wounds International, London, 2010.

[13] S. G. Krzysztof, "Pressure ulcer prevention. Part 1. Causes of pressure ulcers.," *Nursing Times,* vol. 98, no. 11, pp. 41-44, March 2002.

[14] A. Gefen, "The biomechanics of heel ulcers," *Journal of Tissue Viability,* vol. 19, pp. 124-131, 2010.

[15] A. Levy, M. B. Frank and A. Gefen, "The biomechanical efficacy of dressings in preventing heel ulcers," *Journal of Tissue Viability,* vol. 24, no. 1, pp. 1-11, 2015.

[16] R. Katzengolda, M. Topazb and A. Gefen, "Tissue loads applied by a novel medical device for closing large wounds," *Journal of Tissue Viability,* vol. 25, no. 1, p. 32–40, 2016.

[17] H. Mao, X. Jin, L. Zhang, K. H. Yang, T. Igarashi, L. Noble-Haeusslein and A. I. King, "Finite Element Analysis of Controlled Cortical Impact-Induced Cell Loss," *Journal of Neurotrauma,* vol. 27, no. 5, p. 877–888, 2010.

[18] J. G. Snedeker, M. Barbezat, P. Niederer and F. R. Schmidlin, "Strain energy density as a rupture criterion for the kidney: impact tests on porcine organs, finite element simulation, and a baseline comparison between human and porcine tissues.," *Journal of Biomechanics,* vol. 38, no. 5, p. 993–1001, 2005.

[19] V. Luboz, A. Perrier, M. Bucki, B. Diot, F. Cannard, N. Vuillerme and Y. Payan, "Influence of the calcaneus shape on the risk of posterior heel ulcer using 3D patient-specific biomechanical modeling," *Annals of Biomedical Engineering,* vol. 43, no. 2, pp. 325-335, 2015.

[20] A. Levy, K. Kopplin and A. Gefen, "Simulations of skin and subcutaneous tissue loading in the buttocks while regaining weight-bearing after a push-up in wheelchair users," *Journal of the Mechanical Behavior of Biomedical Materials,* vol. 28, pp. 436-447, 2013.

[21] R. Sopher, J. Nixon, E. McGinnis and A. Gefen, "The influence of foot posture, support stiffness, heel pad loading and tissue mechanical properties on biomechanical factors

associated with a risk of heel ulceration," *Journal of the Mechanical Behavior of Biomedical Materials,* vol. 4, no. 4, p. 572–582, May 2011.

[22] P. Kuo, P. Li and M. Li, "Elastic properties of tendon measured by two different approaches," *Ultrasound in Medicine & Biology,* vol. 27, no. 9, p. 1275–1284, September 2001.

[23] B. C. W. Kot, Z. J. Zhang, A. W. C. Lee and et al, "Elastic Modulus of Muscle and Tendon with Shear Wave Ultrasound Elastography: Variations with Different Technical Settings," *Plos One,* vol. 7, no. 8, August 2012.

[24] G. Yarnitzky, Z. Yizhar and A. Gefen, "Real-time subject-specific monitoring of internal deformations and stresses in the soft tissues of the foot: A new approach in gait analysis," *Journal of Biomechanics,* vol. 39, p. 2673–2689, 2006.

[25] I. R. Spears, J. E. Miller-Young, M. Waters and K. Rome, "The effect of loading conditions on stress in the arefooted heel pad," *Medicine and Science in Sports and Exercise,* vol. 37, p. 1030–1036, 2005.

[26] C. Escoffier, J. de Rigal, A. Rochefort, R. Vasselet, J. L. Lévêque and P. G. Agache, "Age-related mechanical properties of human skin: An in vivo study," *The Journal of Investigative Dermatology,* vol. 93, p. 353–357, 1989.

[27] S. Tenenbaum, N. Shabshin, A. Levy, A. Herman and A. Gefen, "Effects of foot posture and heel padding devices on soft tissue deformations under the heel in supine position in males: MRI studies," *JRRD - Journal of Rehabilitation Research and Development,* vol. 50, no. 8, pp. 1149-56, 2013.

[28] E. Linder-Ganz and A. Gefen, "Stress analyses coupled with damage laws to determine biomechanical risk factors for deep tissue injury during sitting," *Journal of Biomechanical Engineering,* vol. 131, no. 1, pp. 011003-011003-13, 2008.

[29] C. E. Clauser, "Weight, volume, and center of mass of segments of the human body," Air Force Systems Command, Wright- Patterson Air Force Base, Ohio, 1969.

[30] T. W. Carey, A. Shaw, M. L. Weber and J. G. DeVine, "Effect of the degree of reverse Trendelenburg position on intraocular pressure during prone spine surgery: a randomized controlled trial," *The Spine Journal,* vol. 14, no. 9, pp. 2118-2126, 2014.

[31] J. R. Boyce, T. Ness, P. Castroman and J. J. Gleysteen, "A preliminary study of the optimal anesthesia positioning for the morbidly obese patient," *Obesity Surgery,* vol. 13, no. 1, pp. 4-9, 2003.

[32] P. Haure, G. E. Cold, T. M. Hansen and J. R. Larsen, "The ICP-lowering effect of 10 degrees reverse Trendelenburg position during craniotomy is stable during a 10-minute period," *Journal of Neurosurgical Anesthesiology,* vol. 15, no. 4, pp. 297-301, 2003.

[33] C. Gould, T. Cull, Y. X. Wu and B. Osmundsen, "Blinded measure of Trendelenburg angle in pelvic robotic surgery," *Journal of Minimally Invasive Gynecology,* vol. 19, no. 4, p. 465–468, 2012.

[34] B. F. Geerts, L. van den Bergh, T. Stijnen, L. P. Aarts and J. R. Jansen, "Comprehensive review: is it better to use the Trendelenburg position or passive leg raising for the initial treatment of hypovolemia?," *Journal of Clinical Anesthesia,* vol. 24, no. 8, pp. 668-674, 2012.

[35] M. A. Borahay, P. R. Patel, T. M. Walsh, V. Tarnal, A. Koutrouvelis, G. Vizzeri, K. Jennings, S. Jerig and G. S. Kilic, "Intraocular pressure and steep trendelenburg during minimally invasive gynecologic surgery: Is there a risk?," *Journal of Minimally Invasive Gynecology,* vol. 20, no. 6, pp. 819-824, 2013.

[36] Standard hospital bed, [Online]. Available: http://www.thecountrycaregroup.com.au/Capri-Bed-4-section-floor-auto-adjust-bed-with-trendelenburg-tilt-P110922.aspx. [Accessed September 2015].

[37] Standard hospital bed, [Online]. Available: http://www.hill-rom.com/usa/Products/Category/Hospital-Beds/Hill-Rom-1000-medical-surgical-bed/ . [Accessed September 2015].

[38] S. Loerakker, E. Manders, G. J. Strijkers, K. Nicolay, F. T. Baaijens, D. L. Bader and C. W. J. Oomens, "he effects of deformation, ischaemia and reperfusion on the development of muscle damage during prolonged loading," *Journal of Applied Physiology,* vol. 111, no. 4, p. 1168–1177, 2011.

[39] B. Pieper, D. Langemo and J. Cuddigan, "Pressure Ulcer Pain: A Systematic Literature Review and National Pressure Ulcer Advisory Panel White Paper," *Ostomy Wound Manage,* vol. 55, no. 2, pp. 16-31, Feb 2009.

[40] US Center of Disease Control and Prevention, National Center for Health Statistics, "The National Nursing Home Survey: 2004 Overview," Series 13, Number 167, June 2009.

[41] A. Gefen, L. H. Cornelissen, D. Gawlitta, D. L. Bader and C. W. Oomens, "The free diffusion of macromolecules in tissue-engineered skeletal muscle subjected to large compression strains," *Journal of Biomechanics,* vol. 41, pp. 845-853, 2008.

[42] A. Gefen, "The biomechanics of heel ulcers," *Journal of Tissue Viability,* vol. 19, no. 4, pp. 124-131, 2010.

Table of Captions

Figure number	Caption	Editing instructions
Figure 1	Heel modeling configuration. (a) Ulcer location in relation to foot posture while in supine position. (b) Part of the MRI image set used for this project. Heel DTI is clearly visible. (c) Finite-element computational model of the heel. (d) Unobscured view of the inner components of the model: the calcaneus and the Achilles tendon (fat and skin layers were made transparent). (e) Mid-sagittal cross section of the heel model, rested on a mattress.	Color is not required for figure in print. This is a 2-column fitting image.
Figure 2	Three mattresses positions used in our work. (a) Mattress in the Trendelenburg position, angle marked by α. $\alpha = 5^o, 10^o, 20^o, 30^o$. (b) A horizontal mattress: $\alpha = \beta = 0^o$. (c) Mattress in the reverse Trendelenburg position, angle marked by β. $\beta = 5^o, 10^o, 20^o, 30^o$.	Color is not required for figure in print. This is a 1.5-column fitting image.
Figure 3	Example of stress and strain distribution in the soft tissues of the heel, rested on a horizontal 80kPa support and loaded by the natural weight of the foot. The original location of the ulcer is marked by a white rectangle. Both sides of the heel are presented. The calcaneus was made transparent for presentation purpose only. (a) Effective stress (Von-Mises) distribution, (b) Lagrangian strain distribution (c) strain energy density distribution. (d) – a zoom-in on the area on the original ulcer location. Extremely high deformations in the fat are clearly visible and indicated by black arrows.	Color is not required for figure in print. This is a 2-column fitting image.
Figure 4	Maximal Effective Stress (kPa) vs. Maximal Shear Stress (kPa) as Function of Mattress Stiffness, FW = 2.2%BW: (a)α - skin,	Color is not required for

	(b)β - skin, (c)α -fat, (d)β – fat. Maximal effective stress in skin vs. fat, as function of the mattress angle: (e) α angle, (g) β angle, Maximal shear stress in skin vs. fat, as function of the mattress angle: (f) α angle, (h) β angle	figure in print. This is a 2-column fitting image.
Figure 5	Maximal Lagrangian strain as function of mattress stiffness, FW = 2.2%BW, for both skin and fat. Angle range for both α and β angles is = 0^o, 5^o, 10^o, 20^o, 30^o. (a) Skin, α. (b) Skin, β. (c) Fat, α. (d) Fat, β.	Color is not required for figure in print. This is a 2-column fitting image.
Figure 6	Maximal Lagrangian strain as function of mattress angle, FW = 2.2%BW, for both skin and fat. Angle range for both α and β angles is = 0^o, 5^o, 10^o, 20^o, 30^o. (a) Skin, α. (b) Skin, β. (c) Fat, α. (d) Fat, β.	Color is not required for figure in print. This is a 2-column fitting image.
Figure 7	Strain energy density distribution in fat and skin vs. effective stress distribution, for various mattress stiffnesses and angles. The calcaneus was made transparent for presentation purpose only. Ulcer location is marked by a dotted square. It is evident that maximal levels of strain energy density are concentrated at the eventual ulcer location.	Color is not required for figure in print. This is a 2-column fitting image.